American Mineralogist, Volume 93, pages 1921–1928, 2008

Pyroxmangite: A high-pressure single-crystal study

P.F. ZANAZZI,[1,*] F. NESTOLA,[2] S. NAZZARENI,[1] AND P. COMODI[1]

[1]Dipartimento di Scienze della Terra, Università di Perugia, Piazza Università, 06100 Perugia, Italy
[2]Dipartimento di Geoscienze, Università di Padova, Via Giotto 1, 35137 Padova, Italy

ABSTRACT

We present the results of a single-crystal X-ray diffraction structural study on pyroxmangite in a diamond-anvil cell up to 5.6 GPa. The sample comes from Yokone-Yama, Awano Town, Tochigi Prefecture, Japan. Crystals are triclinic, centrosymmetric, with composition $[Mn_{0.576(2)}Fe_{0.284(5)}Ca_{0.044(3)}Mg_{0.089(2)}]Si_{1.003(4)}O_3$. Structure refinements were performed with intensity data collected at 1.24 and 3.57 GPa on a CCD-equipped diffractometer. Lattice parameters were accurately measured with the point-detector mounted on the same instrument.

The bulk modulus of pyroxmangite fitting data to a second-order Birch-Murnaghan equation of state is $K_0 = 109.6(7)$ GPa. Axial compressibility values were $\beta_a = 2.2(1)$, $\beta_b = 3.3(1)$, and $\beta_c = 2.6(1)$ 10^{-3} GPa^{-1} showing slightly anisotropic behavior, with the most compressible direction along the *b* axis, as commonly found in the related family of pyroxene.

Silicon tetrahedra are almost incompressible in the pressure range investigated. M polyhedra are more compressible: the volume change is smaller in the more regular octahedra M1–M4 (–3.3%) and greater in the more irregular polyhedra M5–M7 (–5.2%). Owing to the different contraction of Si tetrahedra and cation polyhedra, the sevenfold tetrahedral chains in pyroxmangite must kink to avoid misfit between chains and octahedral bands. This results in shortening of 1.2% of the *c* axis and a decrease in both O_{br} -O_{br}-O_{br} and Si-O_{br}-Si angles.

The behavior of pyroxmangite at high *P* is approximately inverse to that observed at high *T*. Compressibility data may be combined with those on thermal expansion to formulate the approximate equation of state: $V = V_0 (1 - 9.12 \times 10^{-3} \Delta P + 3.26 \times 10^{-5} \Delta T)$, where *P* is in GPa and *T* in degrees Celsius.

Keywords: Pyroxmangite, pyroxenoid, equation of state, compressibility

INTRODUCTION

Pyroxmangite, nominally $MnSiO_3$, is a single-chain silicate belonging to the pyroxenoid polysomatic series, i.e., the series formed by a combination of layers of the two end-member structures—wollastonite (W, Si_3O_9 chains) and clinopyroxene (P, Si_2O_6 chains). Pyroxmangite has the WPP configuration, with a tetrahedral chain of seven Si-O tetrahedra, and is related to rhodonite, which represents the WP configuration, with fivefold chains of Si tetrahedra.

Pyroxmangite was first described by Ford and Bradley (1913), and its crystal structure was determined by Liebau (1959). The structure, like that of pyroxene and other pyroxenoids, may be characterized in terms of approximate closest packing of O atoms, with Si and larger cations filling tetrahedral and pseudo-octahedral sites, respectively. It consists of chains of seven SiO_4 tetrahedra, which alternate with layers of cation-oxygen polyhedra sharing edges. Later, several refinements were carried out on various samples of natural or synthetic pyroxmangite (Ohashi and Finger 1975; Narita et al. 1977; Finger and Hazen 1978; Pinkney and Burnham 1988a) or of the isostructural pyroxferroite (Lindsley and Burnham 1970; Burnham 1971).

The mineral is triclinic, centrosymmetric, and several orientations have been chosen to describe the lattice. The choice of a *C*-centered cell with the chain direction parallel to the *c* axis and the oxygen-closest packing layer parallel to (100), although not canonical, allows better comparisons with clinopyroxene and other pyroxenoids, such as β-wollastonite and rhodonite.

Manganese-rich single-chain minerals are phases forming in various metamorphic assemblages (Peters et al. 1977, 1978; Brown et al. 1980; Winter et al. 1981). Pyroxmangite and rhodonite have been found in blueschist facies conditions in the Alps (Chopin 1978).

Akimoto and Syono (1972) identified four polymorphs of $MnSiO_3$, designated I to IV, in order of increasing pressure and having the structures of rhodonite, pyroxmangite, clinopyroxene, and garnet.

The stability of the pyroxenoids increases from rhodonite to pyroxmangite with increasing *P*, as also demonstrated by the phase relations inferred from field data (Brown et al. 1980). Thermal expansion, compressibility, and chemical substitution effects may be significant in understanding the stability limits of these phases. The effects of temperature on pyroxmangite structure were studied by Pinkney and Burnham (1988b) who also reported a value of compressibility based on lattice parameters measured at 2 GPa. The same authors studied the structural effects of chemical substitutions in pyroxmangite and rhodonite (1988a).

In the present work, we investigate the structural behavior of pyroxmangite at high pressure, making comparisons with

* E-mail: zanazzi@unipg.it

the baric behavior of clinopyroxene. Compressibility data are combined with those on thermal expansion to formulate a *P-V-T* equation of state for pyroxmangite.

Experimental methods

Pale pink crystals of a natural pyroxmangite sample from Yokone-Yama, Awano Town, Tochigi Prefecture, Japan, kindly supplied by Masa Kurosawa (Institute of Geoscience, University of Tsukuba), were selected for high-pressure X-ray diffraction experiments. Their chemical composition was determined at the "Istituto di Geoscienze e Georisorse," CNR Padova (Italy) on a CAMECA-CAMEBAX electron microprobe operating with a fine-focused beam (~1 μm) at an acceleration voltage of 15 kV and a beam current of 15 nA in wave-length dispersive mode (WDS), with 10 s counting times for peaks and 5 s for total background. X-ray counts were converted into oxide wt% with the PAP correction program supplied by CAMECA (Pouchou and Pichoir 1985). Standards, spectral lines and analytical crystals used were: wollastonite for Si and Ca ($K\alpha$, TAP), olivine for Mg ($K\alpha$, TAP), $MnTiO_3$ for Mn ($K\alpha$, LiF), and Fe_2O_3 for Fe ($K\alpha$, LiF). The oxide wt% obtained by averaging about 15 microprobe spots gave the following formula: $[Mn_{0.576(2)}Fe_{0.284(5)}Ca_{0.044(3)}Mg_{0.089(2)}]Si_{1.003(4)}O_3$. The relative oxide wt% values are listed in Table 1.

For refinement at room conditions, a crystal fragment ($0.12 \times 0.08 \times 0.07$ mm in size) was mounted on an XCALIBUR (Oxford Diffr.) diffractometer equipped with both CCD area and point detectors, operating at 50 kV and 35 mA, with graphite monochromated Mo radiation ($\lambda K\alpha_1 = 0.7093$ Å). Diffraction data in the *P* orientation were first collected with the area detector from the crystal in air. To maximize reciprocal space coverage, a combination of ω and φ scans was used, with a step size of 0.8° and a time of 50 s/frame, for a total of 3500 frames. Data were corrected for absorption with the SADABS program (Sheldrick 1996). Details of data collection and refinement are reported in Table 2. The lattice parameters of the $P\bar{1}$ cell were accurately measured with the point detector and calculated by the least-squares fit of Bragg angles for about 40 selected reflections in the θ range 5–25°. Values were converted to the orientation of the $C\bar{1}$ cell for better comparison with the values of Ohashi and Finger (1975) and those determined at high *T* by Pinkney and Burnham (1988b), and are listed in Table 3. The unit cell of the *P* lattice can easily be transformed into the *C* cell by the matrix [$\bar{1}$ $\bar{1}$ 0 | 1 $\bar{1}$ 0 | 0 1 1], and the inverse operation can be carried out with matrix [½ ½ 0 | $\bar{½}$ ½ 0 | ½ ½ 1]. The calculated density, assuming $Z = 4$ in the $C\bar{1}$ cell, is $d_{calc} = 3.745$ g/cm^3. Crystal structure refinement was carried out in the $C\bar{1}$ space group with anisotropic displacement parameters with the SHELX-97 program (Sheldrick 1997), starting from the atomic coordinates of Ohashi and Finger (1975). Neutral atomic scattering factors and $\Delta f'$, $\Delta f''$ coefficients from the *International Tables for Crystallography* (Wilson and Prince 1999) were used. Full occupancy was assumed for all cation sites. The number of electrons in the octahedral cation sites was more than 25 e$^-$ in the M1 site (25.01 e$^-$) and less than 25 e$^-$ in M2–M7 sites (range 22.5–24.2 e$^-$). Therefore, the electronic density in these sites was accounted for by fitting the scattering factor curves of Mn and Fe for site M1, and Mn and Mg for the remaining sites M2–M7, with variable occupancy. The resulting sum of electrons for the octahedral sites in the asymmetric unit of the cell was 167.5 e$^-$, in good agreement with data calculated on the basis of chemical analysis (166.7 e$^-$). At the end of the refinement, no peak larger than 0.6 e$^-$/Å^3 was present in the final difference Fourier synthesis. Table 4[1] lists observed and calculated structure factors. Atomic coordinates and displacement parameters are listed in Table 5.

Table 1. Oxide wt% of the natural sample studied in this work

FeO	MnO	CaO	SiO_2	MgO	Total
16.11	32.38	1.96	47.72	2.85	101.01
0.38	0.29	0.13	0.17	0.07	

Note: Average of 15 analyses and relative standard deviation.

Table 2. Details of data collection and refinement at various pressures

P (GPa)	0.0001*	1.24	3.57
a (Å)	9.663(3)	9.62(1)	9.57(1)
b (Å)	10.457(3)	10.41(1)	10.32(1)
c (Å)	17.360(3)	17.29(1)	17.16(1)
α (°)	112.28(2)	112.0(1)	112.1(1)
β (°)	103.13(2)	103.4(1)	103.2(1)
γ (°)	82.88(2)	83.0(1)	82.9(1)
Volume (Å^3)	1579.4(1)	1559(1)	1528(1)
Space group	$C\bar{1}$	$C\bar{1}$	$C\bar{1}$
θ-range	3–40°	3–30°	3–30°
Crystal-detector distance (mm)	65	65	65
No. measured reflections	12026	7478	8350
No. independent reflections	6334	1316	1156
Reflections with $I > 4\sigma(I)$	4385	894	788
Number of refined parameters	331	142	142
R_{int}%	2.11	9.29	10.2
R_1%	2.22	7.34	6.99

* Data collected with the sample in air.

High-pressure experiments

The pyroxmangite sample was loaded with a chip of Sm^{2+}:BaFCl and a fragment of α-quartz, in an ETH diamond-anvil cell (DAC), equipped with type-I diamonds with 600 μm culet face diameter. The pressure chamber was a 300 μm diameter hole, drilled in a 250 μm thick Inconel 750× gasket preindented to 180 μm. A methanol-ethanol mixture (4:1) was used as hydrostatic pressure-transmitting medium. The wavelength shift of the 6876 Å Sm^{2+} fluorescence line was measured for an approximate estimate of pressure (Comodi and Zanazzi 1993); the quartz crystal was used for precise measurement of pressure (Angel et al. 1997). Uncertainties in pressure calibration based on the equation of state of quartz range between ±0.2 and ±0.8 GPa. Experiments were carried out in the pressure range 10^{-4} to 5.6 GPa (Table 3). Failure of the gasket prevented higher pressures being reached.

The DAC was centered on the diffractometer following the procedure of Budzianowski and Katrusiak (2004). Intensity data were collected with the CCD detector, and the lattice parameters of pyroxmangite and quartz were then accurately measured with the point detector. Several reflections (between 20 and 40) in the θ range 5–28° were used. Several mountings were performed to increase the number of data. Data collected from different crystals yielded a good set of lattice parameters at various pressures (Table 3).

The diffracted intensities from the sample in the DAC are few and of poor quality because of the blind zones due to instrumental limits and occasional overlapping positions with other phases present in the cell, i.e., the two diamonds,

[1] Deposit item AM-08-055, Table 4 (observed and calculated structure factors). Deposit items are available two ways: For a paper copy contact the Business Office of the Mineralogical Society of America (see inside front cover of recent issue) for price information. For an electronic copy visit the MSA web site at http://www.minsocam.org, go to the American Mineralogist Contents, find the table of contents for the specific volume/issue wanted, and then click on the deposit link there.

Table 3. Lattice parameters at various pressures

P (GPa)	*a* (Å)	*b* (Å)	*c* (Å)	α (°)	β (°)	γ (°)	*V* (Å^3)
0.0001	9.663(3)	10.457(3)	17.360(3)	112.28(2)	103.13(2)	82.88(2)	1579.39(6)
0.51	9.643(10)	10.441(7)	17.314(10)	112.13(7)	103.24(8)	82.78(7)	1572.1(3)
0.58	9.648(8)	10.443(6)	17.343(6)	112.30(3)	103.20(6)	82.76(6)	1572.4(2)
0.97	9.643(11)	10.455(6)	17.274(12)	112.22(6)	103.20(9)	82.67(7)	1567.3(2)
2.18	9.609(10)	10.379(10)	17.260(6)	112.26(7)	103.33(6)	82.83(11)	1548.8(2)
2.99	9.596(6)	10.348(6)	17.231(11)	112.34(5)	103.31(6)	82.65(4)	1538.4(2)
3.94	9.582(11)	10.333(11)	17.147(12)	112.28(8)	103.40(8)	82.64(9)	1526.7(4)
4.34	9.569(10)	10.311(9)	17.159(12)	112.26(7)	103.39(8)	82.59(6)	1522.6(4)
4.49	9.576(13)	10.345(12)	17.164(8)	112.20(8)	103.37(7)	82.77(11)	1521.9(4)
4.58	9.549(11)	10.315(12)	17.133(23)	112.20(12)	103.44(11)	82.80(10)	1518.4(4)
4.97	9.544(9)	10.313(10)	17.115(17)	112.16(9)	103.41(9)	82.71(8)	1516.1(4)
5.30	9.553(6)	10.267(8)	17.133(17)	112.23(7)	103.48(7)	82.70(4)	1511.3(4)
5.56	9.544(8)	10.273(8)	17.115(16)	112.33(6)	103.63(6)	82.71(3)	1507.1(4)

TABLE 5. Fractional atomic coordinates and thermal displacement factors U_{eq}/U_{iso} (Å^2) at various pressures

Site	*x*	*y*	*z*	U_{eq}/U_{iso}
M1	−0.00048(3)	0.04202(3)	0.10506(2)	0.0081(1)
	−0.0006(5)	0.0425 (4)	0.1053(3)	0.0097(8)
	0.0010(4)	0.0447(3)	0.1060(2)	0.0080(7)
M2	−0.00031(3)	0.166454(4)	0.31180(2)	0.0084(1)
	−0.0003(5)	0.1667(4)	0.3118(3)	0.0106(9)
	0.0020(5)	0.1664(3)	0.3117(2)	0.0089(8)
M3	0.00061(4)	0.06715(4)	0.60493(2)	0.0078(1)
	−0.0011(5)	0.0664(4)	0.6048(3)	0.0115(8)
	−0.0016(4)	0.0643(3)	0.6040(2)	0.0088(7)
M4	0.01422(4)	0.17658(4)	0.80618(2)	0.0082(1)
	0.0129(5)	0.1771(4)	0.8062(3)	0.0122(9)
	0.0104(5)	0.1766(3)	0.8057(2)	0.0103(8)
M5	0.00392(4)	0.27124(4)	0.51005(2)	0.0112(1)
	0.0045(5)	0.2726(4)	0.5113(3)	0.0169(9)
	0.0056(5)	0.2741(3)	0.5122(2)	0.0134(8)
M6	0.06199(5)	0.26317(4)	0.01728(2)	0.0133(1)
	0.0647(5)	0.2612(4)	0.0159(3)	0.0131(9)
	0.0624(5)	0.2613(4)	0.0161(2)	0.0112(8)
M7	−0.00696(4)	0.37071(4)	0.21006(2)	0.0115(1)
	−0.0060(5)	0.3733(4)	0.2110(3)	0.0155(9)
	−0.0047(5)	0.3747(3)	0.2109(2)	0.0134(8)
Si1	0.20201(6)	0.44251(6)	0.93515(3)	0.0071(1)
	0.1996(9)	0.4431(7)	0.9357(5)	0.011(1)
	0.1981(8)	0.4430(6)	0.9341(4)	0.009(1)
Si2	0.20987(6)	0.33236(6)	0.75112(3)	0.0063(1)
	0.2078(9)	0.3331(6)	0.7515(5)	0.010(1)
	0.2078(8)	0.3295(6)	0.7494(3)	0.007(1)
Si3	0.21097(6)	0.53298(6)	0.66185(3)	0.0066(1)
	0.2118(9)	0.5315(6)	0.6613(5)	0.009(1)
	0.2077(8)	0.5332(6)	0.6613(3)	0.007(1)
Si4	0.20778(6)	0.42495(6)	0.46847(3)	0.0066(1)
	0.2072(9)	0.4256(7)	0.4693(5)	0.012(1)
	0.2063(8)	0.4246(6)	0.4677(3)	0.009(1)
Si5	0.21065(6)	0.63179(6)	0.38004(3)	0.0064(1)
	0.2110(9)	0.6321(6)	0.3800(5)	0.008(1)
	0.2102(8)	0.6355(6)	0.3806(3)	0.007(1)
Si6	0.20935(6)	0.52897(6)	0.18891(3)	0.0067(1)
	0.2097(9)	0.5293(7)	0.1892(5)	0.013(1)
	0.2119(8)	0.5301(6)	0.1893(4)	0.011(1)
Si7	0.20369(6)	0.71058(6)	0.08906(3)	0.0068(1)
	0.2043(9)	0.7119(7)	0.0891(5)	0.009(1)
	0.2058(8)	0.7132(6)	0.0884(4)	0.009(1)
O1	0.1283(2)	0.0728(2)	0.0287(1)	0.0096(3)
	0.132(2)	0.070(1)	0.027(1)	0.012(3)
	0.129(2)	0.071(1)	0.0275(8)	0.005(3)
O2	0.1187(2)	0.1861(2)	0.2267(1)	0.0090(3)
	0.118(2)	0.188(2)	0.227(1)	0.014(3)
	0.122(2)	0.187(1)	0.2264(8)	0.010(3)
O3	0.1179(2)	0.9633(2)	0.3112(1)	0.0091(3)
	0.121(2)	0.964(1)	0.311(1)	0.003(3)
	0.122(2)	0.963(1)	0.3107(9)	0.010(3)
O4	0.1214(2)	0.0896(2)	0.5196(1)	0.0092(3)
	0.123(2)	0.088(1)	0.519(1)	0.012(3)
	0.117(2)	0.088(1)	0.5173(9)	0.015(3)
O5	0.1184(2)	0.8721(2)	0.6057(1)	0.0090(3)
	0.121(2)	0.872(2)	0.607(1)	0.018(3)
	0.118(2)	0.873(2)	0.6051(9)	0.015(3)
O6	0.1209(2)	0.9872(2)	0.8062(1)	0.0091(3)
	0.121(2)	0.987(1)	0.806(1)	0.010(3)
	0.118(2)	0.988(2)	0.8066(9)	0.013(3)
O7	0.1289(2)	0.7800(2)	0.8977(1)	0.0096(3)
	0.132(2)	0.778(1)	0.899(1)	0.014(3)
	0.124(2)	0.777(1)	0.9003(9)	0.012(3)
O8	0.0986(2)	0.8443(2)	0.0938(1)	0.0099(3)
	0.098(2)	0.847(2)	0.094(1)	0.014(3)
	0.103(2)	0.850(1)	0.0934(8)	0.009(3)
O9	0.1284(2)	0.3106(2)	0.9294(1)	0.0125(3)
	0.131(2)	0.309(1)	0.927(1)	0.015(3)
	0.126(2)	0.309(1)	0.9279(9)	0.020(3)
O10	0.1247(2)	0.1962(2)	0.7227(1)	0.0096(3)
	0.122(2)	0.194(1)	0.724(1)	0.014(3)
	0.123(2)	0.192(1)	0.7215(8)	0.013(3)
O11	0.1220(2)	0.6651(2)	0.7117(1)	0.0153(3)
	0.119(2)	0.665(2)	0.713(1)	0.022(4)
	0.114(2)	0.666(1)	0.7130(9)	0.014(3)
O12	0.1228(2)	0.2856(2)	0.4254(1)	0.0136(3)
	0.121(2)	0.286(2)	0.427(1)	0.019(4)
	0.124(2)	0.285(1)	0.4273(8)	0.011(3)
O13	0.1301(2)	0.7758(2)	0.4216(1)	0.0126(3)
	0.135(2)	0.775(1)	0.421(1)	0.013(3)
	0.133(2)	0.779(2)	0.4221(9)	0.015(3)
O14	0.1217(2)	0.3948(2)	0.1318(1)	0.0119(3)
	0.120(2)	0.392(1)	0.133(1)	0.013(3)
	0.126(2)	0.393(1)	0.1313(8)	0.010(3)
O15	0.1654(2)	0.4502(2)	0.8390(1)	0.0097(3)
	0.162(2)	0.451(1)	0.838(1)	0.012(3)
	0.162(2)	0.451(1)	0.8370(9)	0.012(3)
O16	0.1589(2)	0.4032(2)	0.6793(1)	0.0134(3)
	0.156(2)	0.401(1)	0.679(1)	0.010(3)
	0.153(2)	0.400(1)	0.6750(9)	0.014(3)
O17	0.1585(2)	0.4978(2)	0.5604(1)	0.0139(3)
	0.157(2)	0.500(2)	0.562(1)	0.019(4)
	0.152(2)	0.503(1)	0.5604(8)	0.012(3)
O18	0.1499(2)	0.5308(2)	0.4172(1)	0.0128(3)
	0.148(2)	0.529(2)	0.416(1)	0.011(3)
	0.144(2)	0.526(1)	0.4121(9)	0.014(3)
O19	0.1533(2)	0.5672(2)	0.2775(1)	0.0116(3)
	0.152(2)	0.569(1)	0.275(1)	0.011(3)
	0.151(2)	0.572(1)	0.2761(8)	0.009(3)
O20	0.1562(2)	0.6614(2)	0.1592(1)	0.0097(3)
	0.159(2)	0.662(2)	0.158(1)	0.016(4)
	0.161(2)	0.665(1)	0.1598(9)	0.015(3)
O21	0.1429(2)	0.5912(2)	0.9966(1)	0.0101(3)
	0.140(2)	0.592(1)	0.996(1)	0.006(3)
	0.141(2)	0.596(1)	0.9966(8)	0.010(3)

Notes: For each atom values from top to bottom correspond to refinements at 0.0001, 1.24, and 3.57 GPa. The occupancy of Mn against Fe in M1 site in air refined to 0.985(3) atoms; the occupancy of Mn against Mg refined to 0.899(3), 0.917(3), 0.932(3), 0.942(3), 0.807(3), and 0.923(3) atoms for M2, M3, M4, M5, M6, and M7, respectively. Estimated standard deviations refer to the last digit.

powder rings of the beryllium disks, Sm^{2+}:BaClF and quartz used as pressure calibrants. Therefore, in each data collection, the number of reflections suitable for structure refinement was greatly reduced, making the data/parameter ratio very unfavorable for significant results. This is a considerable difficulty when the symmetry of the sample is low, as in the case of pyroxmangite. Therefore, for crystal structure refinements we adopted a different strategy, collecting the data of two crystals coming from the same fragment and with different orientation in the DAC. The pressure of each data collection was evaluated by the previously determined equation of state of pyroxmangite. The two sets of data were corrected for absorption by Absorb V6.1 software (Angel 2004), rescaled and then merged to obtain a larger set of independent data.

Least-squares refinements with data measured at 1.24 and 3.57 GPa, were performed with the SHELX-97 program (Sheldrick 1997). Isotropic atomic displacement parameters were used for all atoms and site occupancies were fixed to the values resulting from the refinement in air. Details of data collections and refinements are listed in Table 2. Observed and calculated structure factors are listed in Table 4, and fractional atomic coordinates and displacement parameters in Table 5.

RESULTS AND DISCUSSION

Compressibility

Unit-cell parameters at various pressures are listed in Table 3 and shown in Figures 1 and 2. The fit of *P-V* data to a third-order Birch-Murnaghan equation of state gives a bulk modulus of K_0 = 111(4) GPa with K' = 3.3(1.7) and V_0 = 1579.40(9) Å^3 (program EOS-FIT V5.2, Angel 2002). However, owing to the *P* range investigated and the quality of the data, a second-order Birch-Murnaghan equation of state (EoS) was the best approximation to describe pyroxmangite volume evolution with *P*, as suggested by plotting "normalized stress" vs. Eulerian finite strain (Jeanloz and Hazen 1991; Angel 2000, 2001) (Fig. 3). The refined EoS parameters were V_0 = 1579.40(8) Å^3, very close to the measured

value (Table 3), and K_0 = 109.6(7) GPa (Fig. 4). Weighted χ^2 was 2.0 and maximum ΔP 0.12 GPa. The present K_0 value differs significantly from that of 87.7 GPa calculated from the volume-compression coefficient with the data measured with only one datum at 20 kbar by Pinkney and Burnham (1988a).

Our bulk modulus value is intermediate between the values of 102 and 117 GPa found for Mn-clinopyroxene and kanoite, respectively (Arlt et al. 1998), and are similar to the values of 113 GPa (K' = 4.8) for diopside (Levien et al. 1979) and 103 GPa (K' = 2) for fassaite (Hazen and Finger 1977).

We determined axial compressibilities by fitting axial compressions (x_{i0}/x_i) to the equation: $\beta_{xi} \cong -1/P \cdot [(x_{i0}/x_i) - 1]$ (where x_i is the selected crystallographic axis, P is pressure, and subscript 0 is ambient pressure) and assuming that β_{xi} are constant in the pressure range of interest (Fig. 1). The data fits between 10^{-4} and 6 GPa yielded β_a = 2.2(1), β_b = 3.3(1), and β_c = 2.6(1) 10^{-3} GPa^{-1}. Therefore the behavior of pyroxmangite, with relative compressions $b > c > a$ in the ratio 1:1.5:1.2, is not far from that of $C2/c$ clinopyroxenes (Thompson and Downs 2008; Zhang et al. 1997). The lattice retains triclinic symmetry over the studied pressure range. Cell angles do not vary significantly, as shown in Figure 2.

Strain ellipsoid

An analysis of the unit-strain tensor (Ohashi 1982) has been performed to better clarify the high-pressure deformation mechanism of pyroxmangite and to compare the results with those of clinopyroxenes. The calculation procedures of the unit-strain tensor are discussed in several previous papers (e.g., Origlieri et al. 2003; Thompson and Downs 2008). The unit-strain ellipsoid size for pyroxmangite calculated between room pressure and 5.56 GPa is ε_1 = –0.0174(2), ε_2 = –0.0323(3), ε_3 = –0.0338(3) GPa^{-1} ($\times 10^2$). The orientations of the strain axes with **a**, **b**, and **c** are as follows: ε_1 ^ **a** = 147.1(5)°, ε_1 ^ **b** = 103.8(8)°, ε_1 ^ **c** = 44.3(5)°; ε_2 ^ **a** = 82(5)°, ε_2 ^ **b** = 27(8)°, ε_2 ^ **c** = 86(7)°; ε_3 ^ **a** = 58(2)°,

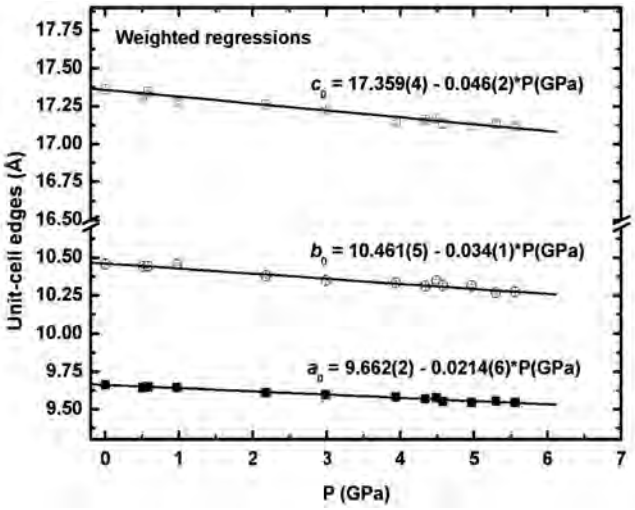

FIGURE 1. Variations in lattice parameters of pyroxmangite as a function of pressure.

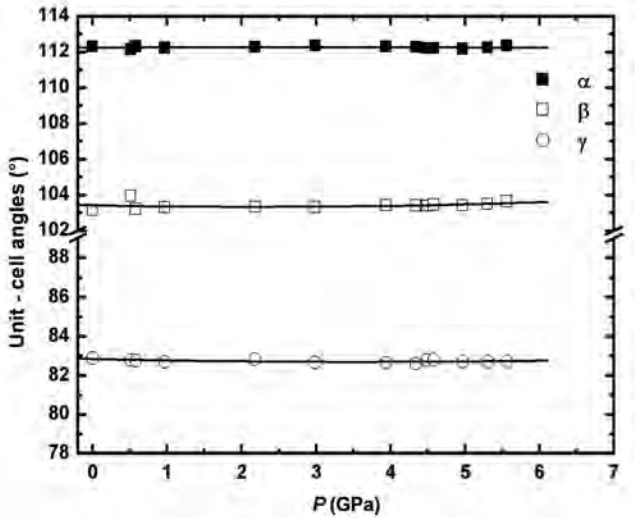

FIGURE 2. Variations of interaxial angles with pressure.

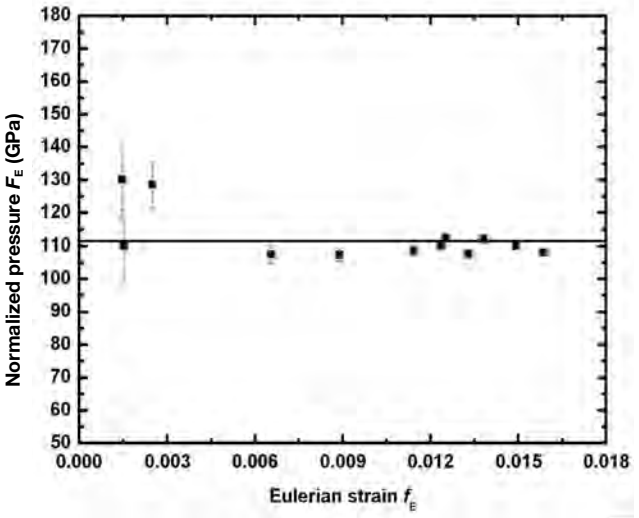

FIGURE 3. Plot of "normalized stress" defined as $F_E = P/[3f_E(1 + 2f_E)^{5/2}]$, vs. finite strain $f_E = [(V_0/V)^{2/3} - 1]/2$.

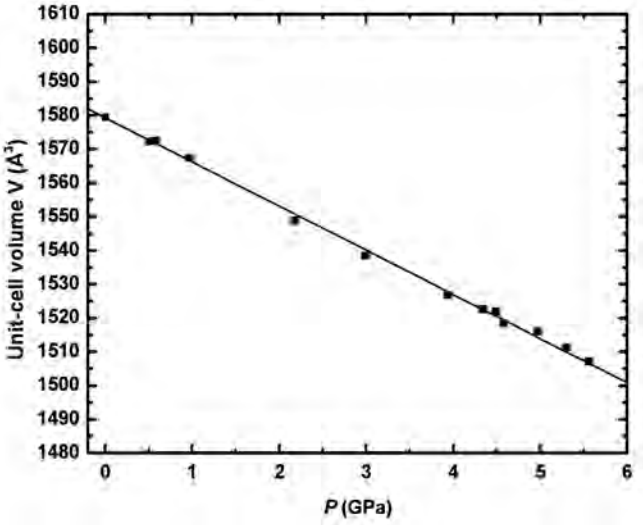

FIGURE 4. Variation in cell volume of pyroxmangite as a function of pressure. The solid line represents the second-order Birch-Murnaghan EoS best fit.

ε_3 ^ **b** = 112(9)°, ε_3 ^ **c** = 46(1)°.

The ellipsoid orientation is very close to that of clinopyroxenes taking into account that pyroxmangite has triclinic symmetry and therefore the ellipsoid is not constrained by any symmetry: for clinopyroxenes ε_2 is coincident with the **b** axis (ε_2 ^ **c** = 90°) and then the other two axes lie on the (0 1 0) plane with the ε_3 ^ **c** usually between 30 and 50° (e.g., Levien et al. 1979; Comodi et al. 1995; Origlieri et al. 2003; Nestola et al. 2006; Thompson and Downs 2008). For pyroxmangite we observe that, within the experimental error, ε_2 is close to the **b** axis, and ε_1 and ε_3 show an orientation closely related to that of clinopyroxenes. Also concerning the magnitude of the three ellipsoid axes we found a fair agreement between pyroxmangite and clinopyroxenes, with ε_1 always the smallest and ε_2 and ε_3 with similar values.

To compare the high-temperature and high-pressure behavior of pyroxmangite we calculated the unit strain for the high-temperature data of Pinkney and Burnham (1988b) between room temperature and 800 °C. Calculations gave the following size and orientations: ε_1 = 0.2835(3), ε_2 = 0.2234(2), ε_3 = 0.09514(2) °C^{-1} ($\times 10^2$). Orientation with respect to the **c** axis was ε_1 ^ **c** = 66.2(8)°, ε_2 ^ **c** = 122.3(8)°, ε_3 ^ **c** = 42.1(4)°. Concerning orientation, note that, whereas ε_1 and ε_2 show very large rotation with respect to the high-pressure orientation, ε_3 is relatively similar to that of our study under pressure. Moreover, at high temperature the three ellipsoid axes show a different scheme with respect to the high-pressure one, ε_3 being the least expansible and ε_1 the most expansible. However, it should be noted that the high-temperature study of Pinkney and Burnham (1988b) was performed on a sample with composition $Mn_{0.97}Mg_{0.02}Ca_{0.01}SiO_3$, and we cannot demonstrate whether the differences in strain ellipsoid size and orientation are due to the changed composition, which in our sample was significantly richer in Fe.

Structural results

The structural results of the pyroxmangite refinement at room pressure match literature data very well (Ohashi and Finger 1975; Pinkney and Burnham 1988a). Tables 6 and 7 list bond distances and relevant geometrical parameters.

The Si-O distances in the tetrahedral chain show the expected bimodal distribution as in the pyroxene structure, with two shorter distances (mean 1.603 Å, range 1.601–1.609 Å) and two longer distances involving bridging O atoms (mean 1.644 Å, range 1.639–1.651 Å). The kinking O-O-O angles formed by bridging O atoms average 160.7°. The mean Si-O_{br}-Si is 136.4°. These values, compared with the homologous values found in diopside [166.4 and 135.8° (Levien and Prewitt 1981); 166.53 and 135.83° (Thompson and Downs 2008)] and in *C*2/*c* $CaMnSi_2O_6$ [164.1 and 137.3° (Nestola et al. unpublished data)] show kinking greater than in clinopyroxene. This is explained by the smaller size of the cation polyhedra in pyroxmangite, requiring contraction of the Si chains.

In pyroxmangite, the first four M cations coordinate six O atoms in almost regular octahedra. The last three M-O polyhedra show more irregular coordination: M5 and M7 have 5 nearer and two farther O atoms (up to 2.90Å), whereas M6 has five shorter and one longer distance (2.781Å) from oxygen. These distorted octahedra are the most probable candidates for hosting Ca, as suggested by Pinkney and Burnham (1988a). M5 has the smallest polyhedral volume (for sixfold coordination) and the greatest angle variance; M6 has the shortest M-O bond length (1.945Å) and is the site preferentially occupied by Mg, in agreement with the occupancy factor resulting from the refinement (Table 5). The mean octahedral M-O distances (Table 6) are intermediate between those found by Ohashi and Finger (1975) for a pyroxmangite with cationic composition $Mn_{0.82}Fe_{0.07}Mg_{0.09}Ca_{0.02}$ and those of pyroxferroite (Burnham 1971) with composition $Mn_{0.02}Fe_{0.83}Mg_{0.02}Ca_{0.13}$ (see Table 42 in Ohashi and Finger 1975). The present values, about 1.5%

TABLE 6. Bond lengths (Å) and relevant angles (°) of pyroxmangite at various pressures

P (GPa)	0.0001	1.24	3.57
Si1-O9	1.590(2)	1.555(17)	1.581(19)
Si1-O1	1.628(2)	1.607(21)	1.646(18)
Si1-O21	1.638(2)	1.638(23)	1.651(17)
Si1-O15	1.657(2)	1.671(20)	1.656(15)
<Si1-O>	1.628	1.618	1.634
Si2-O10	1.588(2)	1.611(17)	1.581(18)
Si2-O2	1.618(2)	1.629(24)	1.594(19)
Si2-O16	1.636(2)	1.617(16)	1.652(15)
Si2-O15	1.665(2)	1.658(26)	1.667(17)
<Si2-O>	1.627	1.629	1.624
Si3-O11	1.592(2)	1.633(27)	1.619(19)
Si3-O3	1.614(2)	1.567(20)	1.587(19)
Si3-O17	1.626(2)	1.594(20)	1.612(15)
Si3-O16	1.655(2)	1.669(17)	1.640(18)
<Si3-O>	1.622	1.616	1.614
Si4-O12	1.597(2)	1.597(18)	1.564(17)
Si4-O4	1.612(2)	1.593(24)	1.648(21)
Si4-O17	1.639(2)	1.653(27)	1.663(18)
Si4-O18	1.642(2)	1.643(15)	1.645(15)
<Si4-O>	1.622	1.621	1.630
Si5-O13	1.592(2)	1.558(24)	1.554(19)
Si5-O5	1.612(2)	1.580(24)	1.603(20)
Si5-O19	1.632(2)	1.656(20)	1.646(15)
Si5-O18	1.649(2)	1.649(19)	1.660(18)
<Si5-O>	1.621	1.610	1.616
Si6-O14	1.590(2)	1.608(17)	1.593(17)
Si6-O6	1.614(2)	1.606(25)	1.604(21)
Si6-O19	1.637(2)	1.602(26)	1.612(17)
Si6-O20	1.642(2)	1.645(16)	1.637(16)
<Si6-O>	1.621	1.615	1.611
Si7-O7	1.591(2)	1.548(23)	1.605(20)
Si7-O8	1.610(2)	1.623(23)	1.602(17)
Si7-O21	1.647(2)	1.652(19)	1.625(15)
Si7-O20	1.656(2)	1.625(23)	1.638(17)
<Si7-O>	1.626	1.612	1.618
M1-O7	2.116(2)	2.143(21)	2.092(17)
M1-O8	2.125(2)	2.095(21)	2.082(15)
M1-O1	2.141(2)	2.168(24)	2.119(16)
M1-O2	2.229(2)	2.222(20)	2.193(16)
M1-O6	2.254(2)	2.241(24)	2.217(17)
M1-O1	2.305(2)	2.287(21)	2.285(15)
<M1-O>	2.195	2.193	2.165
M2-O12	2.072(2)	2.073(20)	2.066(17)
M2-O11	2.113(2)	2.092(20)	2.063(16)
M2-O2	2.146(2)	2.144(26)	2.138(17)
M2-O5	2.194(2)	2.184(25)	2.193(18)
M2-O6	2.241(2)	2.230(20)	2.222(17)
M2-O3	2.282(2)	2.281(19)	2.264(15)
<M2-O>	2.175	2.167	2.158

continued next page

TABLE 6.—*CONTINUED*

P (GPa)	0.0001	1.24	3.57
M3-O13	2.074(2)	2.086(19)	2.049(17)
M3-O10	2.152(2)	2.145(20)	2.124(17)
M3-O4	2.175(2)	2.196(24)	2.162(17)
M3-O3	2.176(2)	2.184(23)	2.174(17)
M3-O5	2.212(2))	2.222(21)	2.164(17)
M3-O4	2.320(2	2.288(21)	2.221(17)
<M3-O>	2.185	2.187	2.149
M4-O10	2.065(2)	2.023(25)	2.051(17)
M4-O6	2.116(2)	2.120(20)	2.090(16)
M4-O9	2.190(2)	2.153(20)	2.155(18)
M4-O20	2.220(2)	2.225(28)	2.186(18)
M4-O3	2.223(2)	2.223(19)	2.192(17)
M4-O8	2.337(2)	2.332(24)	2.356(16)
<M4-O>	2.192	2.179	2.171
M5-O12	2.115(2)	2.080(27)	2.083(17)
M5-O4	2.131(2)	2.147(19)	2.102(16)
M5-O13	2.151(2)	2.184(24)	2.157(19)
M5-O5	2.181(2)	2.207(21)	2.191(17)
M5-O18	2.490(2)	2.485(27)	2.468(18)
M5-O17	2.706(2)	2.688(21)	2.656(19)
M5-O16	2.867(2)	2.814(23)	2.721(17)
<M5-O>[6]	2.295	2.298	2.276
<M5-O>[7]	2.377	2.372	2.340
M6-O14	1.945(2)	1.961(21)	1.937(15)
M6-O9	2.020(2)	2.038(23)	1.987(17)
M6-O1	2.083(2)	2.084(17)	2.059(13)
M6-O8	2.195(2)	2.180(20)	2.197(17)
M6-O21	2.369(2)	2.360(23)	2.311(18)
M6-O7	2.781(2)	2.806(26)	2.679(19)
<M6-O>[5]	2.122	2.124	2.098
<M6-O>[6]	2.232	2.238	2.195
M7-O11	2.096(2)	2.065(25)	2.037(18)
M7-O14	2.135(2)	2.085(25)	2.117(17)
M7-O7	2.144(2)	2.167(20)	2.145(17)
M7-O2	2.229(2)	2.219(20)	2.221(15)
M7-O19	2.476(2)	2.445(20)	2.428(18)
M7-O15	2.546(2)	2.493(19)	2.457(16)
M7-O16	2.900(2)	2.880(28)	2.884(19)
<M7-O>[6]	2.271	2.246	2.234
<M7-O>[7]	2.361	2.336	2.327
Si1-O15-Si2	127.0(1)	126.2(1.1)	125.7(9)
Si2-O16-Si3	135.6(1)	134.2(9)	132.6(1.1)
Si3-O17-Si4	143.8(1)	142.1(1.5)	140.2(1.2)
Si4-O18-Si5	140.4(1)	139.5(1.3)	137.1(1.2)
Si5-O19-Si6	140.2(1)	140.0(1.3)	138.9(1.2)
Si6-O20-Si7	131.5(1)	133.3(1.8)	132.0(1.2)
O21-O15-O16	157.9(1)	158.8(7)	158.4(6)
O15-O16-O17	149.3(1)	147.6(8)	146.3(8)
O16-O17-O18	166.3(1)	164.3(9)	162.0(8)
O17-O18-O19	177.4(1)	176.4(8)	174.0(8)
O18-O19-O20	167.3(1)	168.1(9)	169.4(7)
O19-O20-O21	144.1(1)	144.1(8)	143.9(7)
O20-O21-O15	162.3(1)	162.0(8)	161.3(7)

Notes: Estimated standard deviations refer to the last digit.

TABLE 7. Values of polyhedral volumes (Å^3), and distortion parameters (following Robinson et al. 1971) of tetrahedra and octahedra in pyroxmangite at various pressures

P (GPa)		0.0001	1.24	3.57
Si1	Vol	2.201(15)	2.3(2)	2.2(2)
	λ	1.004	1.016	1.006
	σ^2	15.25	51.9	22.20
Si2	Vol	2.196(15)	2.3(2)	2.2(2)
	λ	1.004	1.010	1.005
	σ^2	17.52	43.17	22.51
Si3	Vol	2.174(15)	2.2(2)	2.1(2)
	λ	1.005	1.005	1.006
	σ^2	20.87	18.07	27.26
Si4	Vol	2.173(15)	2.1(2)	2.2(2)
	λ	1.006	1.006	1.007
	σ^2	24.93	23.02	26.69
Si5	Vol	2.159(15)	2.1(2)	2.1 (2)
	λ	1.009	1.014	1.010
	σ^2	37.47	60.11	41.53
Si6	Vol	2.144(15)	2.0(2)	2.1(2)
	λ	1.013	1.019	1.016
	σ^2	51.20	72.42	60.94
Si7	Vol	2.169(15)	2.0(2)	2.1(2)
	λ	1.012	1.017	1.010
	σ^2	53.01	61.04	44.15
M1	Vol	13.69(3)	12.4(2)	13.2(2)
	λ	1.021	1.019	1.019
	σ^2	63.52(3)	54.37	60.34
M2	Vol	13.41	12.6(2)	13.1(2)
	λ	1.016	1.017	1.018
	σ^2	51.75	56.18	57.43
M3	Vol	13.63(3)	13.1(2)	13.0(2)
	λ	1.014	1.014	1.014
	σ^2	45.50	43.21	46.32
M4	Vol	13.06(3)	12.4(2)	12.7(2)
	λ	1.051	1.056	1.052
	σ^2	173.37	188.40	176.09
M5	Vol	11.92(3)	11.2(2)	11.2(2)
	λ	1.235	1.247	1.264
	σ^2	479.88	510.56	523.45
	Vol [7]	18.01(3)	16.6(2)	17.0(2)
M6	Vol	13.20(3)	12.8(2)	12.6(2)
	λ	1.098	1.099	1.095
	σ^2	249.87	272.73	252.82
	Vol [5]	7.11(3)	7.2(2)	6.9(2)
M7	Vol	14.33(3)	13.7(2)	13.6(2)
	λ	1.065	1.077	1.066
	σ^2	193.62	245.70	200.88
	Vol [7]	17.72(3)	17.1(2)	16.9(2)

Notes: Estimated standard deviations refer to the last digit. λ is the quadratic elongation. σ^2 is the angle variance (°^{2}).

lower than those for the Mn-rich pyroxmangite, i.e., about 30% of the difference in ionic radii of Mn^{2+} and Fe^{2+} (0.82 and 0.78 Å, Shannon 1976), are those expected, in view of the chemical composition of our sample.

Structural evolution with *P*

As expected for silicates, SiO_4 tetrahedra are almost incompressible in the pressure range investigated. The average tetrahedral volume decreases by about 1.4% passing from 2.17 to 2.14 Å^3 at 3.57 GPa (Table 7). M polyhedra are more compressible: their mean volume (for sixfold coordination) decreases from 13.32 to 12.77 Å^3 (about 4.1%). The change is smaller in the more regular octahedra M1–M4 (–3.3%) and greater in the more irregular polyhedra M5–M7, where the longest distances undergo the greatest contraction. This general effect observed in mineral structures at high pressure is explained as due to better packing of O atoms toward close packing with ideal tetrahedral and octahedral coordination.

Owing to the different contraction of SiO_4 tetrahedra and cation polyhedra, the sevenfold tetrahedral chains in pyroxmangite must kink to avoid misfit with the octahedral bands. This results in shortening of 1.2% of the *c* axis and a decrease in the O_{br}-O_{br}-O_{br} angles formed by the bridging O atoms, whose average value passes from 160.7 to 159.3° (–0.9%, Table 6), as well as a decrease in the mean Si-O_{br}-Si angle from 136.4 to 134.6° (–1.3%). The kinking is smaller than that observed at 5.2 GPa in the HP *C*2/*c* polymorph of kanoite, where the O-O-O angle is 140.4° (Arlt et al. 1998).

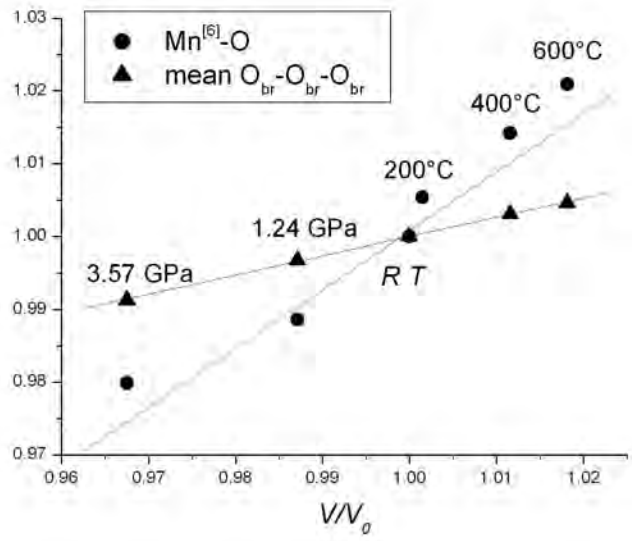

FIGURE 5. Plot of mean octahedral M-O bond length (Å) and of mean O_{br}-O_{br}-O_{br} angle (°) (normalized to room condition values) against normalized unit-cell volumes V/V_0 at various pressures and temperatures (HT values corrected for thermal motion, from Pinkney and Burnham 1988b).

Equation of state

The structural behavior of pyroxmangite at high *P* is only approximately inverse to that observed at high *T*. This is supported by the difference in strain ellipsoids at HP and HT. As an example, in Figure 5 the normalized mean M[6]-O bond lengths and mean O_{br}-O_{br}-O_{br} angles at 1.24 and 3.57 GPa and 200, 400, and 600 °C (values from Pinkney and Burnham 1988b) are plotted against the normalized unit-cell volume (V/V_0), used as a parameter for rescaling the effects of *T* and *P*. The difference between compressibility and expansivity of M sites appears evident.

Compressibility data (β coefficient) may be combined with those on thermal expansion (α coefficient) to formulate an approximate equation of state for the mineral in the *P*-*V*-*T* space. Assuming that the pressure derivative of thermal expansion and the temperature derivative of compressibility are both zero, we can write the equation: $V = V_0 (1 - 9.12 \times 10^{-3} \Delta P + 3.26 \times 10^{-5} \Delta T)$, where *P* is in GPa and *T* in °C. This equation describes structural evolution at various *P*/*T* gradients. For pyroxmangite, the isochoric *P*-*T* path, leaving the structure about equal to that observed in room conditions, is given by ratio β/α and corresponds to 28 °C/kbar. Assuming an average rock density of 2.7 g/cm^3, this is equivalent to a geothermal gradient of 10.4 °C/km, which fits field observations showing that the pyroxmangite structure is stabilized by high-*P*, low-*T* environments (Maresch and Mottana 1976; Chopin 1978; Brown et al. 1980). Clearly this observation only concerns the "geometric" aspect of the structure and does not represent an approach to phase stability in the thermodynamic sense.

ACKNOWLEDGMENTS

This research was supported by Italian MURST grants to P.F.Z. (COFIN 2006–2008, "Studi sperimentali su materiali geologici alle alte pressioni e temperature." We acknowledge the suggestions and comments of the two anonymous referees and the Assistant Editor Przemyslaw Dera.

REFERENCES CITED

Akimoto, S. and Syono, Y. (1972) High pressure transformations in $MnSiO_3$. American Mineralogist, 57, 76–84.

Angel, R.J. (2000) Equation of state. In R.M. Hazen and R.T. Downs, Eds., High-Temperature and High-Pressure Crystal Chemistry, 41, p. 35–59. Reviews in Mineralogy and Geochemistry, Mineralogical Society of America and Geochemical Society, Chantilly, Virginia.

——— (2001) EOS-FIT V6.0. Computer program. Crystallography Laboratory, Department Geological Sciences, Virginia Tech, Blacksburg.

——— (2002) EOS-FIT V5.2. Computer program. Crystallography Laboratory, Department Geological Sciences, Virginia Tech, Blacksburg.

——— (2004) Absorption corrections for diamond-anvil cells implemented in the software package Absorb 6.0. Journal of Applied Crystallography, 37, 486–492.

Angel, R.J., Allan, D.R., Miletich, R., and Finger, L.W. (1997) The use of quartz as an internal pressure standard in high pressure crystallography. Journal of Applied Crystallography, 30, 461–466.

Arlt, T., Angel, R.J., Miletich, R., Armbruster, T., and Peters, T. (1998) High-pressure $P2_1/c$-$C2/c$ phase transitions in clinopyroxenes: influence of cation size and electronic structure. American Mineralogist, 83, 1176–1181.

Brown, P.E., Essene, E.J., and Peacor, D.R. (1980) Phase relations inferred from field data for Mn pyroxenes and pyroxenoids. Contributions to Mineralogy and Petrology, 74, 417–425.

Budzianowski, A. and Katrusiak, A. (2004) High-pressure crystallographic experiments with a CCD-detector. In A. Katrusiak and P. McMillan, Eds., High-pressure Crystallography, p. 101–112. Kluver Academic Publishers, The Netherlands.

Burnham, C.W. (1971) The crystal structure of pyroxferroite from Mare Tranquillitatis. Proceedings of the Second Lunar Science Conference, 1, 47–57.

Chopin, C. (1978) Les paragenèses réduites ou oxydées de concentrations manganésifères des "schistes lustrés" de Haute-Maurienne (Alpes françaises). Bulletin de la Societé Française de Mineralogie et Cristallographie, 101, 514–531.

Comodi, P. and Zanazzi, P.F. (1993) Improved calibration curve for the Sm^{2+}: BaFCl pressure sensor. Journal of Applied Crystallography, 26, 843–845.

Comodi, P., Princivalle, F., Tirone, M., and Zanazzi, P.F. (1995) Comparative compressibility of clinopyroxenes from mantle nodules. European Journal of Mineralogy, 7, 141–149.

Finger, L.W. and Hazen, R.M. (1978) Refined occupancy factors for synthetic Mn-Mg pyroxmangite and rhodonite. Carnegie Institution of Washington, Year Book, 77, 850–853.

Ford, W.E. and Bradley, W.M. (1913) Pyroxmangite, a new member of the pyroxene group and its alteration product, skemmatite. American Journal of Science, 36, 169–174.

Hazen, R.M. and Finger, L.W. (1977) Compressibility and structure of Angra dos Reis fassaite to 52 kbar. Carnegie Institution of Washington, Year Book, 76, 512–515.

Jeanloz, R. and Hazen, R.M. (1991) Finite-strain analysis of relative compressibilities. Application to the high-pressure wadsleyite phase as an illustration. American Mineralogist, 76, 1765–1768.

Levien, L. and Prewitt, C.T. (1981) High-pressure structural study of diopside. American Mineralogist, 66, 315–323.

Levien, L., Weidner, D.J., and Prewitt, C.T. (1979) Elasticity of diopside. Physics and Chemistry of Minerals, 4, 105–113.

Liebau, F. (1959) Über die Kristallstruktur des Pyroxmangits (Mn,Fe,Ca,Mg)SiO_3. Acta Crystallographica, 12, 177–181.

Lindsley, D.H. and Burnham, C.W. (1970) Pyroxferroite: stability and X-ray crystallography of synthetic $Ca_{0.15}Fe_{0.85}SiO_3$ pyroxenoid. Science, 168, 364–367.

Maresch, W.V. and Mottana, A. (1976) The pyroxmangite-rhodonite transformation for the $MnSiO_3$ composition. Contributions to Mineralogy and Petrology, 55, 69–79.

Narita, H., Koto, K., and Morimoto, N. (1977) The crystal structures of $MnSiO_3$ polymorphs (rhodonite- and pyroxmangite-type). Mineralogical Journal of Japan, 8, 329–342.

Nestola, F., Boffa Ballaran, T., Liebske, C., Bruno, M., and Tribaudino, M. (2006) High-pressure behavior along the jadeite $NaAlSi_2O_6$-aegirine $NaFeSi_2O_6$ solid solution up to 10 GPa. Physics and Chemistry of Minerals, 33, 417–425.

Ohashi, Y. (1982) A program to calculate the strain tensor from two sets of unit-cell parameters. In R.M. Hazen and L.W. Finger, Eds., Comparative Crystal Chemistry, p. 92–102. Wiley, New York.

Ohashi, Y. and Finger, L.W. (1975) Pyroxenoids: A comparison of refined structures of rhodonite and pyroxmangite. Carnegie Institution of Washington, Year Book 74, 564–569.

Origlieri, M.J., Downs, R.T., Thompson, R.M., Pommier, C.J.S., Denton, M.B., and Harlow, G.E. (2003) High-pressure crystal structure of kosmochlor, $NaCrSi_2O_6$, and systematics of anisotropic compression in pyroxenes. American Mineralogist, 88, 1025–1032.

Peters, T., Valarelli, J.V., Coutinho, J.M.V., Sommerauer, J., and von Raumer, J. (1977) The manganese deposits of Buritirama (Para, Brazil). Schweitzerisches

Mineralogie Petrographie Mitteilungen, 57, 313–327.
Peters, T., Schwender, H., Tromsdorff, V., and Sommerauer, J. (1978) Manganese pyroxenoids and carbonates: Critical phase relations in metamorphic assemblages from the Alps. Contributions to Mineralogy and Petrology, 66, 383–388.
Pinkney, L.R. and Burnham, C.W. (1988a) Effects of compositional variation on the crystal structures of pyroxmangite and rhodonite. American Mineralogist, 73, 798–808.
——— (1988b) High temperature crystal structure of pyroxmangite. American Mineralogist, 73, 809–817.
Pouchou, J.L. and Pichoir, F. (1985) PAP phi-rho-Z procedure for improved quantitative microanalysis. In J.L. Armstrong, Ed., Microbeam Analysis, p. 104–106. San Francisco Press, Inc., California.
Robinson, K., Gibbs, G.V., and Ribbe, P.H. (1971) Quadratic elongation, a quantitative measure of distortion in coordination polyhedra. Science, 172, 191–193.
Shannon, R.D. (1976) Revised effective ionic radii and systematic studies of interatomic distances in halides and chalcogenides. Acta Crystallographica, A32, 751–767.
Sheldrick, G.M. (1996) SADABS. Program for empirical absorption correction of area detector data. Institut für Anorganische Chemie, University of Göttingen, Germany.
——— (1997) SHELX-97. Program for crystal structure determination and refinement. Institut für Anorganische Chemie, University of Göttingen, Germany.
Thompson, R.M. and Downs, R.T. (2008) The crystal structure of diopside at pressure to 10 GPa. American Mineralogist, 93, 177–186.
Wilson, A.J.C. and Prince, E. (1999) International Tables for X-ray Crystallography, Volume C: Mathematical, Physical and Chemical Tables, 2nd edition. Kluwer Academic, Dordrecht.
Winter, G.A., Essene, E.J., and Peacor, D.R. (1981) Carbonate and pyroxenoids from the manganese deposit near Bald Knob, North Carolina. American Mineralogist, 66, 278–289.
Zhang, L., Ahsbahs, H., Hafner, S.S., and Kutoglu, A. (1997) Single-crystal compression and crystal structure of clinopyroxene up to 10 GPa. American Mineralogist, 82, 245–258.

Manuscript received February 26, 2008
Manuscript accepted June 19, 2008
Manuscript handled by Przemyslaw Dera